ChemPubSoc Europe

DOI: 10.1002/cssc.201802016

CHEMSUSCHEM Full Papers

Structural Design of Ionic Liquids for Optimizing Aromatic Dissolution

Haihui Joy Jiang,[a] Silvia Imberti,[b] Blake A. Simmons,[c, d] Rob Atkin,[e] and Gregory G. Warr*[a]

Certain protic ionic liquids (PILs) are potentially low-cost, high-efficiency solvents for the extraction and processing of aromatic compounds. To understand the key design features of PILs that determine solubility selectivity at the atomic level, neutron diffraction was used to compare the bulk structure of two PILs with and without an aromatic solute, guaiacol (2-methoxyphenol). Guaiacol is a common lignin residue in biomass processing, and a model compound for anisole- or phenol-based food additives and drug precursors. Although the presence of amphiphilic nanostructure is important to facilitate the dissolution of solute nonpolar moieties, the local geometry and competitive interactions between the polar groups of the cation, anion, and solute are found to also strongly influence solvation. Based on these factors, a framework is presented for the design of PIL structure to minimize competition and to enhance driving forces for the dissolution of small aromatic species.

Introduction

Lignin is an abundant and renewable source of high-value chemicals, such as vanillin and a wide variety of anisole-based and phenolic products.[1] These aromatic species are important food additives and drug precursors.[2] Ionic liquids (ILs) have recently emerged as effective solvents for lignin extraction and aromatic dissolution.[3] The current benchmark, 1-ethyl-3-methylimidazolium acetate (EmimOAc), has a good yield, but is not economically viable, owing to its high cost (>USD 50 per kg) and processing temperatures above 100 °C.[4] ILs currently finding use in the chemical industry combine protic cations with a mineral acid anion[3a] to form protic ionic liquids (PILs), which are an order of magnitude cheaper. Both secondary and tertiary alkylammonium PILs performed comparably to EmimOAc for lignin extraction, but at a fraction of the cost (USD 1.25 kg^{-1}),[5] although monoethylammonium PILs were found to be less effective. In addition, PILs have advantages of low toxicity, high biocompatibility, and water tolerance, which are desirable characteristics as processing solvents.[6]

Our understanding of the mechanisms underlying the extraction of aromatics with PILs is in its infancy. Using lignin extraction as an example, the performance of PILs is usually considered, like molecular solvents, in terms of solvent polarity or anion basicity, but these average indicators do not account for molecular-level factors that are hypothesized to control the solubility of individual residues in PILs.[7] Most PILs have an amphiphilic nanostructure consisting of polar and non-polar domains that percolate through the liquid.[8] The solubility of aromatic species in PILs will depend on interactions between its aromatic rings and their substituents with either the polar and apolar phases, which are completely unexplored at the molecular level. This means that pathways to optimizing ion structures cannot be identified rationally.

In this work, we used neutron diffraction to compare the solution structure of guaiacol (2-methoxyphenol),[9] in two PILs at the molecular level. The PILs selected for study are propylammonium nitrate (PAN), which has a primary cation, and pyrrolidinium acetate (PyrrAc), which comprises a secondary cation, and is one of the more promising PIL lignin solvents due to its high extraction yield and low processing temperature.[3b] Guaiacol is fully miscible in both PILs. The molecular structure of guaiacol is representative of aromatic components of lignin, which contain *p*-hydroxyphenyl, guaiacol, and syringyl units,[10] and lignin depolymerization products from different treatment methods.[11] Guaiacol is also representative of many substituted small aromatic compounds such as anisole, aniline, anethole, and other phenol derivatives. Structural understanding of how these small aromatics dissolve in PILs has broad applicability in designing task-specific solvents for aromatic dissolution and biomass processing. Table S1 and S2 (see the Supporting Infor-

[a] H. J. Jiang, Prof. G. G. Warr
School of Chemistry and Sydney Nano Institute
The University of Sydney, NSW 2006 (Australia)
E-mail: gregory.warr@sydney.edu.au

[b] Dr. S. Imberti
STFC, Rutherford Appleton Laboratory
Didcot OX11 0QX (UK)

[c] Dr. B. A. Simmons
Biological Systems and Engineering Division
Lawrence Berkeley National Laboratory
1 Cyclotron Rd., Berkeley, CA, 94720 (USA)

[d] Dr. B. A. Simmons
Deconstruction Division, Joint BioEnergy Institute
5885 Hollis St., Emeryville, CA, 94608 (USA)

[e] Prof. R. Atkin
School of Molecular Sciences
The University of Western Australia
35 Stirling Hwy, WA 6009 (Australia)

Supporting Information and the ORCID identification number(s) for the author(s) of this article can be found under: https://doi.org/10.1002/cssc.201802016.

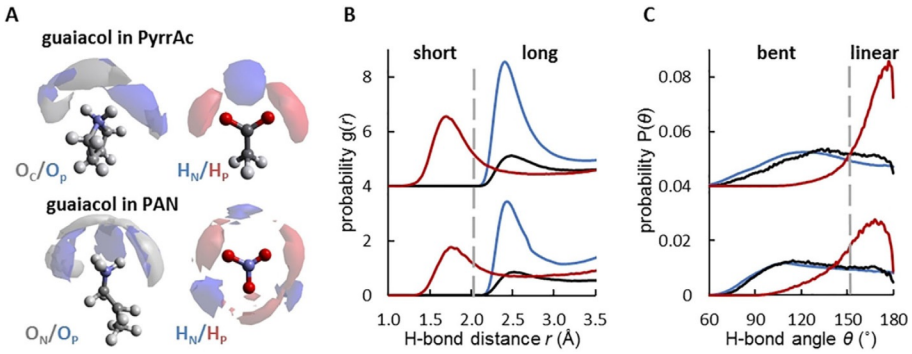

Figure 1. Key H-bonding atomic arrangements for 25 wt% guaiacol in PyrrAc (top) and PAN (bottom). Three interactions are color-coded: cation–anion (blue), cation–guaiacol (black), and anion–guaiacol (red). A) 20% probability surfaces for the competitive arrangement of H-bond acceptors of the anion (O_C on acetate or O_N on nitrate) and phenol oxygen (O_p) of guaiacol around cations (left), and complementary arrangement of H-bond donors from the ammonium cation (H_N) and guaiacol phenol (H_p) around the anions (right). B) Corresponding bond length and C) bond angle distributions, distinguishing short, straight bonds from long, bent bonds.

mation) show the molecular structures of solute and solvent with atomic labels used throughout this work.

Neutron diffraction with hydrogen/deuterium isotopic substitution (Table S1 and Figure S1) yields multiple contrasts for each chemical system. The liquid nanostructure of pure PAN[12] and PyrrAc[13] have been described previously. PAN has a pronounced liquid nanostructure and well-defined ion arrangements. PyrrAc also exhibits an amphiphilic nanostructure, but the ion arrangements within the structure are less well defined than for PAN. In this study, we have examined solutions of guaiacol in PyrrAc at 10 and 25 wt%, and in PAN at 10 wt%. The atomic arrangements within the liquid were found to be independent of concentration (Figure S2), although better statistics were achieved at 25 wt%. This method unambiguously determines the locations of hydrogen atoms and the corresponding part of the molecule in a sample, enabling the identification of intermolecular interactions that drive dissolution. By using empirical potential structure refinement (EPSR) to model and simultaneously fit solutions with identical chemical compositions but different H/D substitutions (Table S2 and S3 and Figure S1), liquid structure is determined with near-atomic resolution. We will correlate IL geometry, H-bonding capacity, and amphiphilicity to solvent performance.

Results and Discussion

Solvent–solute interactions in the polar region

In both PAN–guaiacol and PyrrAc–guaiacol, the dominant correlations are between polar groups on the cation (RNH_3^+ or $R_2NH_2^+$), the anion ($RCOO^-$ or NO_3^-) and the guaiacol phenol group, all of which are capable of H-bonding (Figure S2). Figure 1 compares the details of hydrogen bond arrangements for guaiacol in PyrrAc (top row) and in PAN (bottom row).

Figure 1 A shows the spatial arrangements of the most probable 20% of H-bond acceptors around cations and H-bond donors around anions. The H-bond acceptors of the anion and phenol oxygen of guaiacol[1] form two lobes above and around $Pyrr^+$ and three lobes around PA^+. However, there is essentially no difference between the locations of phenol and the anion acceptor atoms, which compete for the cation. In contrast, the H-bond donors of the ammonium cation (H_N) and guaiacol phenol (H_p) occupy different spatial locations around both nitrate and acetate anions. In PyrrAc, the cation charged group is preferentially located between anion oxygens due to electrostatics, so the H_N atoms form a lobe in this region. This leaves H-bonding positions available near each donor O_C, resulting in two symmetrical lobes corresponding to linear H-bonds to H_p. This is also clearly seen in the H-bond angle distribution (Figure 1 C), which is sharply peaked near 180° for the anion–guaiacol correlation, whereas bond angle distributions of anion and guaiacol phenol around the cation are both less well-defined, with broad peaks at 90–150°.

The same behavior is seen around nitrate in PAN, but with threefold symmetry. The cation H-bond donors lie between O_N, whereas the guaiacol occupies the vacant linear positions. The peak at 180° in Figure 1 C is less pronounced.

Partial pair correlation functions (Figure 1 B) show that linear anion-guaiacol preferred bond length of 1.7 Å is also much shorter than both the cation-anion and cation-guaiacol H-bond lengths of 2.4–2.5 Å, indicating a much stronger interaction (a statistical summary of H-bond properties is given in Tables S4 and S5). This is similar to previous results for H-bonding in pure primary alkylammonium PILs.[14] The competition for H-bonding sites around the cation, but differences around the anion, is consistent with earlier reports that the species of the anion is more important than the cation for biomass dissolution.[15]

Solvent–solute interactions in the apolar region

Both PyrrAc and PAN are amphiphilically nanostructured liquids,[12,13] which is a property known to enhance miscibility with alkanols.[16] The structure of their apolar domains may therefore contribute to the miscibility of guaiacol with both

[1] *The participation of the methoxy group in hydrogen bonding is much less than that of the phenol group (Figure S2)*

PyrrAc and PAN. Pair correlation functions (Figure S3) indicate relatively strong associations between the terminal carbons of propylammonium cations and weak associations between the bottom carbons (C_2) of pyrrolidinium and with the aromatic ring of guaiacol. Figure 2 shows the most probable locations of both the terminal methyl of the cation (C_3) and the center of mass of the guaiacol aromatic ring (Ar) around a representation of the propylammonium cation. The C_3 methyl locations are consistent with the bulk liquid structure of PAN,[12] in which the alkyl chains of the cation segregate into a tail-to-tail or bilayer-like sponge arrangement. The guaiacol aromatic ring occupies similar, albeit less well-defined, positions, consistent with its solubilization into apolar regions.

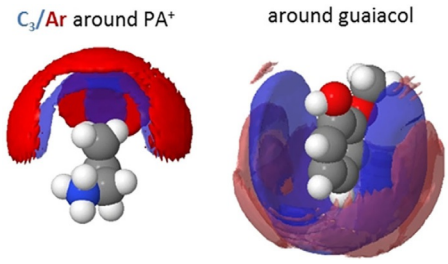

Figure 2. The most probable geometric arrangements between the PA^+ alkyl tail (blue) and the guaiacol aromatic ring (red).

Figure 3 shows the relative distribution of the centers of mass of pyrrolidinium and guaiacol apolar rings as a function of distance and orientation. As seen in pure PyrrAc,[13] the distribution of $Pyrr^+$ rings is almost independent of angular orientation, suggesting no preferred alignment or stacking of cations. The spatial probability distribution of $Pyrr^+$ rings is similarly homogeneous, but also highlights the amphiphilic association of these non-polar groups into domains segregated from the polar ammonium cation and acetate anion. In contrast, guaiacol-guaiacol correlations show a strong propensity for face-to-face (parallel) stacking of aromatic rings. Surprisingly, $Pyrr^+$–guaiacol ring correlations also exhibit a preferred parallel alignment. This is likely to be a packing preference of the planar guaiacol ring, considering the absence of strong intermolecular interactions. Such steric constraints may also underpin the preferential orientation of guaiacol rings. In contrast to PAN, the absence of preferential orientation of the $Pyrr^+$ rings in the apolar domain means that they can solvate the guaiacol and rearrange into a favorable conformation with minimal energetic cost.

Solvent nanostructure

Figure 4 A and B show representative snapshots of the EPSR simulation of 10 wt% guaiacol in PyrrAc and PAN, respectively, converged to the experimental neutron diffraction patterns, with IL polar head groups, apolar hydrocarbons and guaiacol molecules labelled in different colors. PAN displays a sponge-like bicontinuous solvent structure with near-equal volumes of interpenetrating polar and non-polar domains. In PyrrAc, apolar groups take up the major volume, forming a continuous apolar domain. The liquid structures are consistent with those

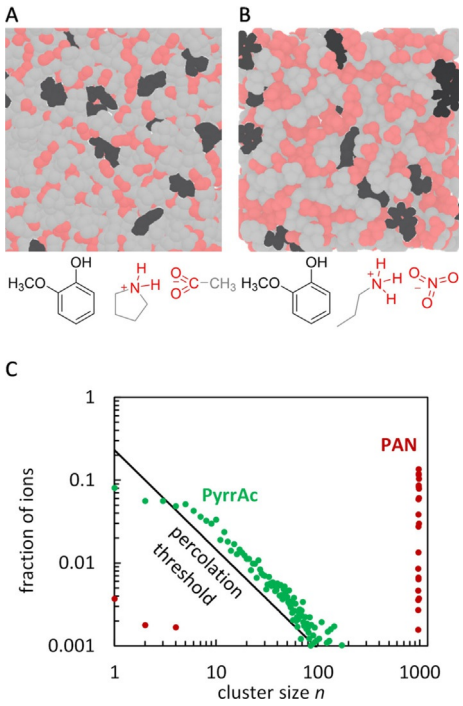

Figure 4. A, B) Snapshots of converged simulation boxes of PyrrAc–guaiacol (A) and PAN–guaiacol (B); color coding distinguishes IL polar groups (red), IL apolar hydrocarbons (grey), and guaiacol (black). C) Cluster analysis of IL polar groups, defined by H-bond distance < 2.8 Å. Theoretical percolation threshold $= n^{-1.2}/4.34$, derived from probabilities (see Ref. [18]).

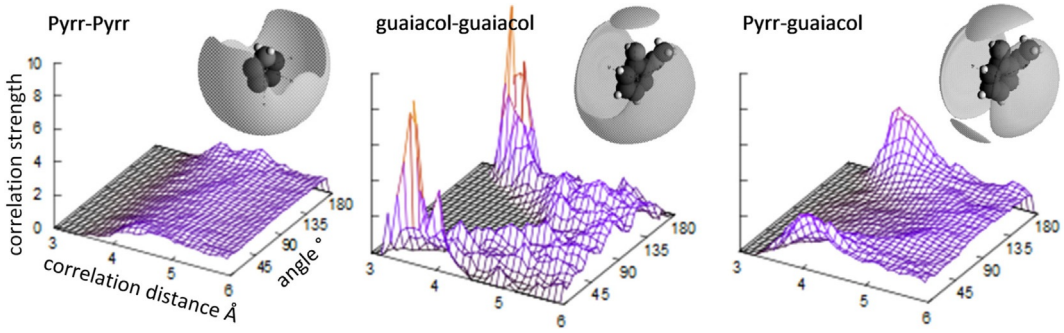

Figure 3. Ring–ring angular distribution maps, derived from the angle between the normal of two rings and the distance between geometric centers.

previously reported for pure PAN and PyrrAc.[12,13] In both ILs, guaiacol is evenly distributed throughout the solvent with no segregation and is in contact with both the polar and the apolar domains, as inferred from the preceding analysis.

The extent of the H-bond network may be quantified by cluster analysis (Figure 4C), which reveals the fraction of ions in a cluster of size *n*, consisting of nearest neighbors within cation–anion H-bond range (< 2.8 Å, from Figure 1). Whereas PyrrAc exhibits a distribution of finite clusters close to that expected for a random percolation threshold, PAN almost exclusively forms clusters that span the simulation box, indicating a continuous H-bonding network of ammonium and nitrate ions. The dense, three-dimensional H-bond network of PAN with three donors and three acceptors per ion pair stabilizes the continuous polar network. In PyrrAc, with only two donors and two acceptors, no such network forms. This parallels the H-bonding conditions required for molecular solvents to exhibit a solvophobic effect and induce micelle formation.[17]

Considerations for aromatic dissolution

Although solvent nanostructure is a desirable feature that provides suitable polar and apolar solvent microenvironments for guaiacol and other similar solutes with polar and nonpolar groups, the details of H-bond donor and acceptor availability are also critical. Primary alkylammonium cations favor an extended H-bond network within the polar domains of the liquid which is not possible for secondary or tertiary alkylammonium species. This allows incorporation of the solute's polar moieties into the polar domains without disrupting the existing solvent H-bond network. ILs can act as designer solvents because their nanostructure is driven by electrostatics, allowing H-bond availability to be tuned independently. This explains why secondary (including PyrrAc) and tertiary ammonium PILs are more effective solvents than corresponding primary ammonium PILs for lignin extraction.[5,19]

The H-bonding capacity of the anion is also an important factor to consider. Both nitrate and acetate provide distinct acceptor sites that can simultaneously accommodate short, straight phenolic and long, bent ammonium cation H-bond donors (Figure 1A). Our previous study, which showed that ethylammonium thiocyanate and hydrogensulfate themselves form dense networks of short, straight cation–anion H-bonds,[14] suggests that they should not be effective solvents for guaiacol, as is observed.[5]

There is little difference between the apolar domain sizes of a cyclic secondary ammonium (PyrrAc) or a primary ammonium cation (PAN). While relatively small for ILs, they are large enough to accommodate small aromatic moieties like guaiacol. To dissolve solutes with larger non-polar groups, we anticipate that ILs with longer aliphatic chains (i.e. matched with the solute) to be better performing.[16a] However, increasing the cation alkyl chain length leads to better-defined cation alkyl chain packing in apolar domains.[20] This is contrary to the disordered packing in PyrrAc and is important for its solvency power. Therefore, strategies for increasing the apolar volume without increasing order such as mixtures of cations with different alkyl chain lengths[21] or branched chains should be pursued.

Conclusions

Our study highlights the importance of the anion–guaiacol interaction for solubilization. Acetate is a good anion for guaiacol solubilization, owing to its asymmetry and site-specific interactions with the solute. To optimize the solubilization of phenolic compounds or alike, we hypothesize that reducing the number of H-donors on the cation will minimize competing interactions between the cation and phenyl groups and therefore enhance the anion–solute interaction. This hypothesis was validated by using $Pyrr^+$ (with fewer H-donors than PA^+), which was found to be a more effective cation. This approach is also supported by the observation that aromatic solubilization decreases following the order of triethylammonium > diethylammonium > ethylammonium.[5]

Our results indicate that a matched amphiphilicity between the solvent and the solute is a minimum criterion for the solubilization of small aromatic species. For all the ILs studied, the cation determined solvent amphiphilicity. Pyrrolidinium and propyl- and branched alkylammonium species all contain a polar head group and apolar hydrocarbon tails or rings. ILs containing one of these cations can solubilize anisole-based and phenolic species and are potential extraction solvents for aromatic polymers such as lignin. Beyond this basic amphiphilicity requirement, the extent of IL nanostructure is less relevant to the extraction efficiency based on our current observations.

We note finally that the practical application of ILs will frequently take place in the presence of water, whether adventitious or deliberately-added. Water dissolution has been shown to modify the H-bonding network structure in protic ILs, while leaving the amphiphilic nanostructure largely intact.[22] Water content may thus be an additional variable that can be used to tune the competition for H-bonding sites on aromatic or other organic residues. This is currently under further investigation.

Experimental Section

PyrrAc and PAN were synthesized by acid-base neutralization from appropriate concentrated reagents as described previously.[12,13] After drying, water contents were below 0.6 wt% and following neutron diffraction experiments (after two months storage and shipping) did not exceed 0.9 wt%. Chemically identical but isotopically different contrasts for each PIL were made. Guaiacol (either hydrogenous or deuterated) was added to each PIL to form binary mixtures at 10 and 25 wt% (Tables S1 and S2).

Neutron diffraction was performed on the SANDALS diffractometer at 298 K (Rutherford Appleton Laboratories, UK), with structure factors extracted as described by Soper et al.[23] Empirical potential structure refinement (EPSR) was used to model the PIL–guaiacol bulk structures.[24] All systems contain over 1000 ions and molecules with box size over $45\times45\times45$ Å^3. The model iterates a Monte Carlo framework that is refined against the measured dif-

fraction data, as well as other liquid parameters (Table S3 and Figure S1).

Acknowledgements

The authors acknowledge financial support from the Australian Research Council, and HJJ the receipt of a Henry Bertie and Florence Mabel Gritton Research Scholarship from the University of Sydney. We gratefully acknowledge the Science and Technology Facilities Council (STFC) for access to neutron beamtime at ISIS.

Conflict of interest

The authors declare no conflict of interest.

Keywords: ionic liquids · nanostructures · neutron scattering · noncovalent interactions · solvents

[1] a) "Deconstruction of lignocellulosic biomass to fuels and chemicals": S. P. S. Chundawat, G. T. Beckham, M. E. Himmel, B. E. Dale in *Annual Review of Chemical and Biomolecular Engineering, Vol. 2* (Ed.: J. M. Prausnitz), Annual Reviews, Palo Alto, CA, **2011**, pp. 121 – 145; b) P. Varanasi, P. Singh, M. Auer, P. D. Adams, B. A. Simmons, S. Singh, *Biotechnol. Biofuels* **2013**, *6*, 14; c) K. Stärk, N. Taccardi, A. Bösmann, P. Wasserscheid, *ChemSusChem* **2010**, *3*, 719 – 723.

[2] a) R. G. Berger, *Aroma Biotechnology*, Springer, Berlin, Heidelberg, **1995**, pp. 1 – 10; b) A. A. Salim, Y.-W. Chin, A. D. Kinghorn in *Bioactive Molecules and Medicinal Plants* (Eds.: K. G. Ramawat, J. M. Merillon), Springer, Berlin, Heidelberg, **2008**, pp. 1 – 24.

[3] a) A. Brandt, J. Grasvik, J. P. Hallett, T. Welton, *Green Chem.* **2013**, *15*, 550 – 583; b) E. C. Achinivu, R. M. Howard, G. Q. Li, H. Gracz, W. A. Henderson, *Green Chem.* **2014**, *16*, 1114 – 1119.

[4] a) A. Brandt, J. P. Hallett, D. J. Leak, R. J. Murphy, T. Welton, *Green Chem.* **2010**, *12*, 672 – 679; b) N. Sun, M. Rahman, Y. Qin, M. L. Maxim, H. Rodriguez, R. D. Rogers, *Green Chem.* **2009**, *11*, 646 – 655; c) A. Pinkert, D. F. Goeke, K. N. Marsh, S. Pang, *Green Chem.* **2011**, *13*, 3124 – 3136.

[5] A. George, A. Brandt, K. Tran, S. Zahari, D. Klein-Marcuschamer, N. Sun, N. Sathitsuksanoh, J. Shi, V. Stavila, R. Parthasarathi, S. Singh, B. M. Holmes, T. Welton, B. A. Simmons, J. P. Hallett, *Green Chem.* **2015**, *17*, 1728 – 1734.

[6] C. G. Yoo, Y. Q. Pu, A. J. Ragauskas, *Curr. Opin. Green Sustainable Chem.* **2017**, *5*, 5 – 11.

[7] R. Hayes, G. G. Warr, R. Atkin, *Chem. Rev.* **2015**, *115*, 6357 – 6426.

[8] H. J. Jiang, R. Atkin, G. G. Warr, *Curr. Opin. Green Sustainable Chem.* **2018**, *12*, 27 – 32.

[9] J. B. Binder, M. J. Gray, J. F. White, Z. C. Zhang, J. E. Holladay, *Biomass Bioenergy* **2009**, *33*, 1122 – 1130.

[10] A. J. Ragauskas, G. T. Beckham, M. J. Biddy, R. Chandra, F. Chen, M. F. Davis, B. H. Davison, R. A. Dixon, P. Gilna, M. Keller, P. Langan, A. K. Naskar, J. N. Saddler, T. J. Tschaplinski, G. A. Tuskan, C. E. Wyman, *Science* **2014**, *344*, 1246843.

[11] C. Xu, R. A. Arancon, J. Labidi, R. Luque, *Chem. Soc. Rev.* **2014**, *43*, 7485 – 7500.

[12] R. Hayes, S. Imberti, G. G. Warr, R. Atkin, *Phys. Chem. Chem. Phys.* **2011**, *13*, 13544 – 13551.

[13] H. J. Jiang, S. Imberti, R. Atkin, G. G. Warr, *J. Phys. Chem. B* **2017**, *121*, 6610 – 6617.

[14] R. Hayes, S. Imberti, G. G. Warr, R. Atkin, *Angew. Chem. Int. Ed.* **2013**, *52*, 4623 – 4627; *Angew. Chem.* **2013**, *125*, 4721 – 4725.

[15] A. George, K. Tran, T. J. Morgan, P. I. Benke, C. Berrueco, E. Lorente, B. C. Wu, J. D. Keasling, B. A. Simmons, B. M. Holmes, *Green Chem.* **2011**, *13*, 3375 – 3385.

[16] a) H. J. Jiang, P. A. FitzGerald, A. Dolan, R. Atkin, G. G. Warr, *J. Phys. Chem. B* **2014**, *118*, 9983 – 9990; b) T. Murphy, R. Hayes, S. Imberti, G. G. Warr, R. Atkin, *Phys. Chem. Chem. Phys.* **2016**, *18*, 12797 – 12809; c) T. L. Greaves, D. F. Kennedy, N. Kirby, C. J. Drummond, *Phys. Chem. Chem. Phys.* **2011**, *13*, 13501 – 13509.

[17] A. Ray, *Nature* **1971**, *231*, 313 – 315.

[18] N. Jan, *Phys. A* **1999**, *266*, 72 – 75.

[19] G. F. De Gregorio, C. C. Weber, J. Grasvik, T. Welton, A. Brandt, J. P. Hallett, *Green Chem.* **2016**, *18*, 5456 – 5465.

[20] R. Hayes, S. Imberti, G. G. Warr, R. Atkin, *J. Phys. Chem. C* **2014**, *118*, 13998.

[21] Z. F. Chen, T. L. Greaves, G. G. Warr, R. Atkin, *Chem. Commun.* **2017**, *53*, 2375 – 2377.

[22] R. Hayes, S. Imberti, G. G. Warr, R. Atkin, *Angew. Chem. Int. Ed.* **2012**, *51*, 7468 – 7471; *Angew. Chem.* **2012**, *124*, 7586 – 7589.

[23] A K. Soper, W. S. Howells, A. C. Hannon, *ATLAS: Analysis of Time-of-Flight Diffraction Data from Liquid and Amorphous Samples*. Rutherford Appleton Laboratory, Didcot, **1989**.

[24] A. K. Soper, *Chem. Phys.* **1996**, *202*, 295.

Manuscript received: August 31, 2018
Revised manuscript received: October 3, 2018
Accepted manuscript online: October 9, 2018
Version of record online: November 9, 2018